

See discussions, stats, and author profiles for this publication at: <https://www.researchgate.net/publication/235248104>

Atmospheric reactivity of CH₂ICl with OH radicals: High-level OVOS CCSD(T) calculations for the x-abstraction pathways (X = H, Cl, or I)

ARTICLE in THE JOURNAL OF PHYSICAL CHEMISTRY A · JANUARY 2013

Impact Factor: 2.69 · DOI: 10.1021/jp312447x

CITATIONS

6

READS

39

4 AUTHORS:



Katarina Sulkova

Faculty of Materials Science and Technology S...

9 PUBLICATIONS 33 CITATIONS

SEE PROFILE



Martin Šulka

Slovak University of Technology in Bratislava

7 PUBLICATIONS 33 CITATIONS

SEE PROFILE



Florent Louis

Université des Sciences et Technologies de Lill...

45 PUBLICATIONS 401 CITATIONS

SEE PROFILE



Pavel Neogrady

Comenius University in Bratislava

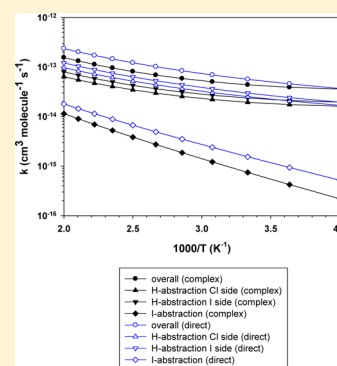
50 PUBLICATIONS 2,671 CITATIONS

SEE PROFILE

Atmospheric Reactivity of CH₂ICl with OH Radicals: High-Level OVOS CCSD(T) Calculations for the X-Abstraction Pathways (X = H, Cl, or I)Katarína Šulková,[†] Martin Šulka,[†] Florent Louis,^{*,‡} and Pavel Neogrády^{*,†}[†]Department of Physical and Theoretical Chemistry, Faculty of Natural Sciences, Comenius University, Mlynská dolina CH1, 84215 Bratislava, Slovakia[‡]PhysicoChimie des Processus de Combustion et de l'Atmosphère (PC2A), UMR 8522 CNRS/Lille1, Université Lille 1 Sciences et Technologies, Cité Scientifique, Bât. C11/C5, 59655 Villeneuve d'Ascq Cedex, France

S Supporting Information

ABSTRACT: Reactants, weak molecular complexes, transition states, and products for the H-, Cl-, and I-abstraction channels in the reaction of OH radicals with chloriodomethane CH₂ICl as well as the energy profiles at 0 K have been determined using high-level all-electron ab initio methods. The results showed that all-electron DK-CCSD(T)/ANO-RCC approach performed very well in predicting the reactivity of iodine. In terms of activation enthalpy at 0 K, the energy profile for the Cl-abstraction showed that this reaction pathway is not energetically favorable in contrast to the two other channels (H- and I-abstractions), which are competitive. The H-abstraction was strongly exothermic (−87 kJ mol^{−1}), while the I-abstraction was modestly endothermic (11.8 kJ mol^{−1}). On the basis of our calculations including the following corrections to the potential energies: basis set saturation, valence and core–valence electron correlation, relativistic effects, spin-adaptation, vibration contributions, and tunneling corrections, rate constants were predicted using canonical transition state theory over the temperature range 250–500 K for each abstraction pathway. The overall rate constant at 298 K was estimated to be 4.29×10^{-14} and 5.44×10^{-14} cm³ molecule^{−1} s^{−1} for complex and direct abstraction mechanisms, respectively. In addition, the overall rate constant computed at 277 K was used in the estimation of the atmospheric lifetime for CH₂ICl. On the basis of our theoretical calculations, the atmospheric lifetime for the OH removal process is predicted to be close to 1 year. In terms of atmospheric lifetime, the OH reaction is not competitive with the Cl reaction and photolysis processes.



1. INTRODUCTION

Researches conducted over the last four decades, spurred by the discovery of methyl iodide (CH₃I) in the atmosphere by Lovelock et al.,¹ have shown that most of the organic iodine in the atmosphere is coming from the ocean (see, for example, reviews by Vogt,² Cicerone,³ Chameides and Davis,⁴ Carpenter,⁵ and Saiz-Lopez et al.⁶). In addition to CH₃I, other iodine-containing organics (larger alkyl iodides and multiple halogenated methanes such as CH₂I₂ and CH₂ICl) have been also identified in ambient air and/or ocean water. In the case of the CH₂ICl compound, it has been also identified in marine boundary layer (MBL) air and/or in surface seawater.^{7–16} Recently, laboratory data showed that a new and purely chemical volatile source was independent of biological generation and depends on the presence of atmospheric ozone, dissolved iodide, and dissolved organic matter.¹⁷ Total fluxes of iodine to the atmosphere are uncertain but are thought to be on the order of hundreds of Gg per year.¹⁸ The only non-negligible anthropogenic sources appear to be emission from rice paddies¹⁹ and possibly biomass burning.^{11,20–22} The mechanisms involved in the production of these iodine-containing species in the ocean focused on either the production of methyl iodide by algae and phytoplankton^{4,9,23,24} or the possibility of photochemical production in ocean water.^{25–27} Even though

numerous estimates have been made of the flux of methyl iodide from the ocean to the atmosphere,^{4,23,28–30} less is known about CH₂ICl. Various measurements^{7,8,10} have shown seawater concentrations of CH₂ICl in the northwestern Atlantic to be comparable to or greater than those of CH₃I. Sources may be from phytoplanktonic and/or Cl[−] substitution reactions.⁸ The potential importance in coastal regions was shown by Carpenter et al.¹¹ Algae appear to constitute also a source of multihalogenated species.^{12,31}

Iodine in its various forms is rapidly converted to iodine atoms. Iodine chemistry may influence tropospheric HO₂/OH and NO₂/NO concentration ratios and hence the oxidizing capacity of the atmosphere.^{4,32} The iodine chemistry may play an important role in the destruction of ozone.³³ Calvert and Lindberg³⁴ performed computer simulations on the tropospheric chemistry of iodine-containing compounds in the polar spring. Their results showed potential enhancement of ozone depletions through the presence of iodine-containing molecules (I₂, IBr, ICl, CH₂I₂, CH₂IBr, CH₂ICl, and CH₃I).

Received: October 8, 2012

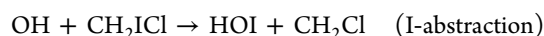
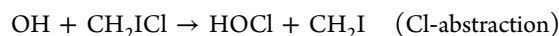
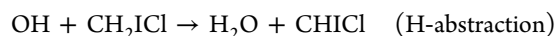
Revised: January 7, 2013

Published: January 7, 2013



Atmospheric loss processes for iodoalkanes include photolysis and gas-phase reactions with OH radicals and Cl atoms. Rate coefficient data for reaction of OH with iodoalkanes have been experimentally determined for a series of alkyl iodides (CH_3I ,^{35–37} $\text{C}_2\text{H}_5\text{I}$,^{37,38} $1\text{-C}_3\text{H}_7\text{I}$,^{37–39} and $2\text{-C}_3\text{H}_7\text{I}$,^{37–39}) as well as for CH_2I_2 .³⁸ Most of these data have been also collected in two recent books dealing with the atmospheric chemistry of halogenated species.^{18,40} Literature data suggest the expected trend, an increase in the rate coefficient with increasing size of the alkyl iodide. Rate coefficients for other multiply halogenated species (CH_2ICl and CH_2IBr) are not currently available although Orlando¹⁸ estimated their reactivity to be small toward OH radicals.

All iodine-containing organic compounds possess fairly strong absorption features in the near-ultraviolet, and many of these species have a quantum yield near unity for photo dissociation to release an iodine atom.⁴¹ The atmospheric photo dissociation rates of CH_2ICl have been investigated^{42,43} and showed that photolysis is a fast process with tropospheric lifetimes of an order of a few hours. To assess the role played by CH_2ICl in atmospheric chemistry, kinetic and mechanistic information concerning their reactions with atmospherically relevant species such as OH radicals and Cl atoms is needed. The kinetics and mechanism of Cl atoms with CH_2ICl has been already studied.^{44,45} The rate constant data for reaction of OH with CH_2ICl are not available in the literature, although Orlando¹⁸ estimated the value to be less than $10^{-13} \text{ cm}^3 \text{ molecule}^{-1} \text{ s}^{-1}$ at 298 K. In partial fulfillment of this need, we report here the results of a theoretical study of the reactivity of OH radicals toward CH_2ICl considering all possible abstraction channels:



High-level ab initio molecular orbital studies offer a viable alternative to provide reliable kinetic data for the gas-phase reactions. Modeling abstraction from iodine-containing organic compounds is a rather demanding task because, for predicting the kinetic parameters, one has to reach at least the chemical accuracy. This implies to choose the computational chemistry tools that include all necessary and accurate corrections to molecular energies^{46,47} (basis set saturation, valence and core–valence electron correlation, relativistic effects, spin-adaptation, vibration contributions, and tunneling corrections).

In this article, we will report the results of ab initio calculations obtained for the H-, Cl-, and I-abstraction reactions of OH radicals with chloriodomethane CH_2ICl . Typically, the potential energy surface for the bimolecular gas-phase abstraction reaction can be simplified to the double-well energy profile with two minima corresponding to molecular complexes either on the reactant side (MCR) or on the product side (MCP) separated by the transition state (TS). Special emphasis must be paid to the choice of efficient theoretical methods that can provide a quantitative and balanced description of each stationary point on the potential energy surface of this process. To the best of our knowledge, this is the first time that the reactivity of OH radicals with CH_2ICl has been studied.

2. METHODOLOGY AND COMPUTATIONAL DETAILS

The stationary points on the reaction profile (reactants, molecular complexes, and transition states) were determined using gradient optimizations with the second-order perturbation theory employing the Møller–Plesset partitioning of the Hamiltonian (MP2).^{48,49} We have used in the geometry optimizations Dunning's triple- ζ correlation consistent basis set cc-pVTZ for light atoms⁵⁰ and Peterson's pseudo potential basis set of the same class on iodine.⁵¹ All optimizations (including the frequency check) were performed with the Gaussian03 program.⁵² The ab initio vibrational frequencies were multiplied by an appropriate scaling factor (0.950).⁵³ Special care was taken to determine minimum energy pathways (MEPs), performing intrinsic reaction coordinate analyses (IRC)^{54,55} at the MP2/cc-pVTZ level of theory, in order to confirm that specific TS connects the different local minima. The two electronic states for OH radical are included in the calculation of its electronic partition function, with a 139.21 cm^{-1} splitting⁵⁶ in the $^2\Pi$ ground state.

Single-point energy calculations at all the stationary points of the reaction profile were performed using the coupled cluster theory including single, double, and noniterative triple substitutions (CCSD(T)) in the basis of canonical orbitals as implemented in the MOLCAS7.0 program.⁵⁷ This is an efficient parallel version of the CC-code, based on the restricted open-shell Hartree–Fock reference (ROHF). Since the CCSD procedure brings some spin contamination into the final wave function, we have used a simple spin-adaptation scheme of the dominant DDVV part of T_2 excitation amplitudes, leaving the T_1 excitation amplitudes nonadapted.^{58,59} Diagonal Fock matrix elements were used as denominators in the calculation of the triples contribution to the CCSD energy. For heavy atoms like iodine, one has to include at least the scalar relativistic effects in the calculation.^{60,61} The second-order spin-free Douglas–Kroll–Hess Hamiltonian^{62,63} was applied to calculate scalar relativistic effects within the CCSD(T). This leads to the one-component spin-adapted approach, DK-CCSD(T). The respective code is implemented in MOLCAS7.0.

Two types of relativistic contraction of the ANO-RCC primitive sets for H(8s4p3d1f), C/O(14s9p4d3f2g), Cl-(17s12p5d4f2g), and I(22s19p13d5f3g) were adopted. The first one corresponds to the valence quadruple- ζ contraction for H, C, O, and Cl atoms: H[4s3p2d1f], C/O[5s4p3d2f1g], and Cl[6s5p3d2f1g]. In the second contraction, we used the large contraction on iodine atom: I[10s9p8d5f2g].⁶⁴ Of course, to use the full large contraction for all atoms would be a better approach, but already the trade-off with the large set for iodine atom is at the limit of our computational resources. The ANO-RCC sets allow correlation of the 4d electrons on iodine; this automatically includes the important part of the semicore correlation in our calculations. In order to minimize the possible basis set superposition error (BSSE), we have applied the modification of the Boys–Bernardi^{65,66} counterpoise (CP) correction as proposed by Xantheas.⁶⁷ This modification includes also the geometry relaxation when going from the subsystems to the supersystem. The CP correction is applicable to weakly interacting molecular complexes but not to TS, where it can lead to discontinuous potential surfaces.⁶⁸ Therefore, we will use the CP correction just as an estimate of the error bars for reaction barriers.

The evaluation of BSSE using a modified scheme with geometry relaxation involves three times more calculations for

each subsystem, making the BSSE calculations very demanding. In order to reduce the computational costs, we have used the OVOS (optimized virtual orbital space) method with controlled accuracy.⁶⁹

The main idea of the OVOS method, introduced originally by Adamowicz et al.^{70,71} and reformulated later by Neogr dy et al.⁷² is to perform specific unitary transformation of the virtual orbital space in which we try to accumulate most of the flexibility of the complete virtual orbital space (VOS) into selected smaller subspace. In subsequent correlation calculations, we use only this truncated set of optimized virtual orbitals, which should reproduce the flexibility of the whole set of VOS. The remaining part of VOS is deleted from the calculations, what makes OVOS based computational schemes significantly less time-consuming. The optimization criterion for selecting the truncated virtual space is the maximum overlap of the first-order perturbative wave functions in the full and reduced virtual space. The application of the OVOS technique is similar to FNO (frozen natural orbitals) approach,^{73–75} which can be considered as an approximation of the OVOS method.⁷⁶

In most of the OVOS applications, we need to evaluate MP2 energy both with full VOS and in reduced OVOS sets. Adamowicz et al.^{70,71} showed that the accuracy of the highly correlated OVOS based calculations is significantly improved when treating MP2 terms in complete VOS. It is useful to employ the so-called Y_2 correction⁷⁷ defined as a difference between MP2 energy in the full and reduced VOS, respectively:

$$Y_{2,MP2} = MP2^{Full} - MP2^{OVOS} \quad (1)$$

The total energy is then defined as a sum of CCSD(T) energy calculated in reduced VOS and the Y_2 correction

$$CCSD(T)_2^{OVOS} = CCSD(T)^{OVOS} + Y_{2,MP2} \quad (2)$$

That means only post-MP2 terms are calculated in truncated VOS. The performance of OVOS was shown in several previous works.^{57,72,76–78} Obviously, when the quality of reduced OVOS approaches complete VOS, $Y_{2,MP2}$ comes to zero. This parameter can be, in general, viewed as an indicator of the accuracy of OVOS approach. As was shown recently by Kraus et al.,⁶⁹ the errors in post-MP2 terms, $Y_{2,post-MP2}$, are closely related to $Y_{2,MP2}$. In the chemically interesting region of errors, where $Y_{2,MP2}$ error is above 1 μ Hartree, it was observed that the size of the $Y_{2,post-MP2}$ errors can be controlled on the basis of the following inequalities:

$$\log|Y_{2,MP2}| \geq \log|Y_{2,CCSD-MP2}| \quad (3)$$

$$\log|Y_{2,MP2}| \geq \log|Y_{2,CCSD(T)-MP2}| \quad (4)$$

These relations can be used for specific application of the OVOS method for more efficient evaluation of BSSE, where OVOS is applied exclusively to the subsystems.^{69,79} Reducing the VOS to the size of the subsystem in BSSE calculations, we typically encounter an error of 10^{-5} – 10^{-4} a.u. Dependence of the $\log|Y_{2,MP2}|$ value on the size of virtual space, so-called " $Y_{2,MP2}$ error profile", can be obtained relatively easy for every studied system. From these error profiles, we can easily determine the size of the virtual space needed to reach a given accuracy (10^{-5} a.u. in this work), which is negligible compared to the absolute value of the CP correction itself. Figure 1 illustrates the procedure how one can obtain truncated OVOS from $Y_{2,MP2}$ profiles of subsystems for the iodine abstraction

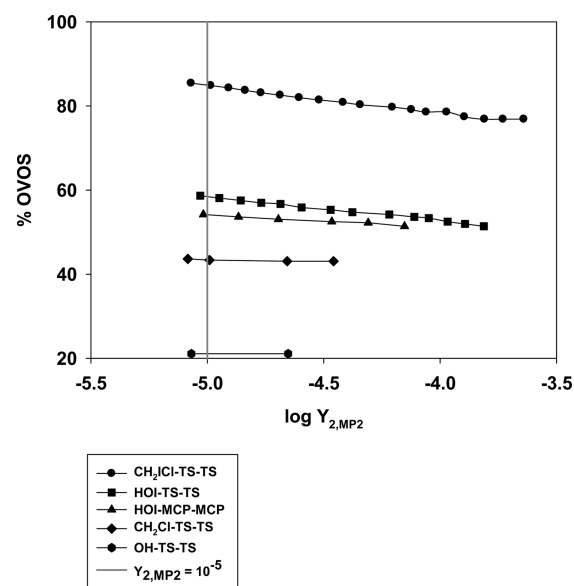


Figure 1. $Y_{2,MP2}$ error profiles of subsystems from I abstraction channel. Notation in legend stands for system-basis-geometry.


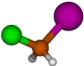
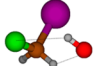
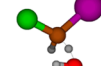
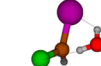
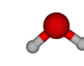
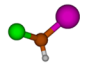
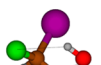
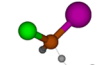
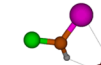
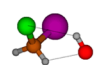
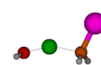
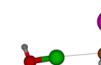
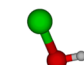

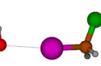
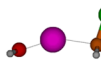
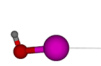

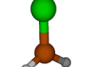
pathway. It is obvious that the error profile of each individual subsystem is different depending on the size of the system. Virtual space of the CH₂ICl, the largest considered subsystem, calculated in supermolecular basis (TS) can be reduced only to about 85%, but CH₂Cl to ~45% and OH up to ~20% of the full virtual orbital space. It corresponds to speed up of factor 2, 25, and 625 for CH₂ICl, CHCl, and OH, respectively.

Further, we can see that error profiles of the same system differ also depending on the supersystem in which they have been calculated. For example, VOS of HOI calculated in supermolecular basis of MCP can be reduced to a larger extent than if calculated in the TS supermolecular basis. This can be due to the more compact character of TS, from which then we cannot delete so many orbitals.

It is evident, that the method of direct controlling of the absolute value of the error in the OVOS method, described recently by Kraus et al.,⁶⁹ is slightly different compared to the traditional concept of OVOS applications. In typical OVOS calculations, we try to keep an absolute error of the method constant, but not necessarily negligible. Overall applicability of the OVOS procedure is dependent on the mutual error cancellation because final properties are always differences between absolute energies. Thus, we try to balance the size of the VOS reduction to produce approximately the same error of all involved species. This is typically ensured by reducing VOS to the same percentage of the overlap functional in all calculations.^{76–78} In a specific case of BSSE calculations, we can, however, achieve chemically negligible absolute energy errors for subsystems (in supersystem basis) even with significantly reduced OVOS. Thus, we can perform supersystem calculations in full basis set and subsystems within OVOS approach and subtract these values without affecting the accuracy of the BSSE correction. The results of our calculations show that the OVOS profile is copying the one calculated in full VOS and holds virtually the same accuracy along the entire energy profile, all differences being within 0.1 to 0.15 kJ mol⁻¹.

Though the CCSD(T) approach is considered as a golden standard, providing a good balance between cost and accuracy, it is still possible to improve the CC energies estimating the

Table 1. Molecular Configurations and Spin–Orbit Corrections to the Calculated Potential Energies in kJ mol^{-1} for Species Involved in This Work

OH	CH ₂ ICI	MCR _{Hab,ClSide}	TS _{Hab,ClSide}	MCP _{Hab,ClSide}	H ₂ O	CHICI
						
−0.83	−2.73	−2.57	−2.17	−2.60		−2.75
		MCR _{Hab,Iside}	TS _{Hab,Iside}	MCP _{Hab,Iside}		
						
		−2.57	−2.05	−2.27		
		MCR _{Clab}	TS _{Clab}	MCP _{Clab}	HOCl	CH ₂ I
						
		−2.56	−2.23	−1.21	−0.49	−2.30
		MCR _{Iab}	TS _{Iab}	MCP _{Iab}	HOI	CH ₂ Cl
						
		−3.09	−4.20	−5.65	−5.94	−0.02

effects of higher excitations, i.e., the FCI energies as proposed by Goodson.⁸⁰ This is referred to as continued fraction approximation (cf). The method works quite well even for stretched bonds, typical for TS, and is applicable for molecules with smooth convergence in CCSD. We will apply cf-correction in the energetics of each studied pathway.

Inclusion of spin–orbit coupling (SOC) is important for reactivity of iodine.^{47,81–83} We used the restricted active space state interaction method (CASSCF/CASPT2/RASSI-SO,⁸⁴ shortly CASPT2/RASSI-SO) in conjunction with the second order multiconfigurational perturbation theory (CASPT2), employing the complete active space (CASSCF) wave function as a reference. The second-order spin-free Douglas–Kroll–Hess Hamiltonian was applied to calculate the scalar relativistic effects within the CASPT2 method. To reduce the computational effort with a negligible loss of accuracy, we used atomic mean field integrals (AMFI). All calculations reported have been done using the MOLCAS7.0 package. SOC effects were included as an a posteriori correction, using one-electron Fock-type spin–orbit Hamiltonian to approximate the SOC operator.

The values of the spin–orbit corrections to the calculated potential energies for all stationary points are collected in Table 1. An inclusion of SO effects in the case of OH radical leads to splitting of the ground state of OH ($^2\Pi_i$) and lowering the energy by $-0.833 \text{ kJ mol}^{-1}$. The calculated correction is in excellent agreement with the values either from Huber⁵⁶ or Hess et al.⁸⁵ ($-0.833 \text{ kJ mol}^{-1}$) and with the literature value from the NIST-JANAF thermochemical database⁸⁶ ($-0.836 \text{ kJ mol}^{-1}$). Considering the remaining species, the SO coupling between the ground state and the excited states is almost quenched, due to the large energy separation between them. In such cases, we consider the energy shift due to the residual SOC stabilization or simply second-order SO effect. There are no literature data available for the stationary points collected in Table 1 except for the molecule HOI. In this case, our

calculated SO correction for HOI ($-5.94 \text{ kJ mol}^{-1}$) is larger than the one obtained by Stevens et al.⁸⁷ using the one-electron effective spin–orbit Hamiltonian ($-1.69 \text{ kJ mol}^{-1}$). This is mainly because of different level of theory and active space used in the calculations ((6e/5o) of active space by Stevens et al.⁸⁷ contrary to our (10e/7o) active space), as well as different optimized geometries.

As it can be seen in Table 1, the SO corrections for molecular complexes (MCR and MCP) are close to the ones obtained for either reactants or products. The difference between these values does not exceed $1\text{--}2 \text{ kJ mol}^{-1}$. According to the Hammond's postulate,⁸⁸ the structure of the transition state depends on the exothermicity/endothermicity of the reaction. When the reaction is exothermic, the transition state structure is rather similar to reactants (reactant-like), while in the case of endothermic reaction, it is more product-like. It seems that spin–orbit splitting of the TS obeys the same rule. It can be best observed in the I-abstraction pathway where the differences in SO splitting of reactants, TS, and products are the biggest ones. Since this pathway is slightly endothermic (see section 3.), the TS structure should be product-like, and we can expect a comparable effect of SO as for products. This is clearly shown in Table 1 where we present also the molecular configurations of stationary points together with their corresponding SO corrections. The geometries of TS and MCP look like the ones of the products, the values of SO correction for TS and MCP approach the one of the HOI molecule. The conclusion is that if one does not want to calculate values of SO corrections for all the stationary points, then it is acceptable to calculate only SO effects for reactants/products and the values of MCR, MCP, and TS are approximated by corresponding values keeping in mind the Hammond's postulate. Adopting such strategy will lead to results without significant loss of accuracy and big computational savings.

The rate coefficient k for the different abstraction pathways involves a hydrogen-bonded adduct. It was initially analyzed according to the scheme advocated by Singleton and Cvetanovic⁸⁹ for prereactive complexes. We assume here that the reaction occurs according to the following two-step mechanism:



involving a fast pre-equilibrium between the reactants and the prereactive complex MCR, followed by an abstraction leading to the postreactive complex and the products. For steady-state conditions applied to reactions (a–c), the effective reaction rate r is

$$r = r_c = k[\text{OH}][\text{CH}_2\text{ICl}] \quad (\text{5})$$

where k is the overall rate constant for each studied pathway following the above mechanism.

k can be written as

$$k = \frac{k_a k_b}{(k_b + k_c)} \quad (\text{6})$$

Even though the energy barrier for k_b is about the same size as that for k_c , the entropy change is much larger in the reverse reaction (b) than in the reaction (c) going to the transition state. Thus, k_b is expected to be considerably larger than k_c , and k can be rewritten as

$$k = \frac{k_a k_b}{k_c} = K_{a,b} k_c \quad (\text{7})$$

where $K_{a,b}$ is the equilibrium constant between the isolated reactants and the prereactive complex MCR. Applying basic statistical thermodynamics principles for the calculation of the equilibrium constant of the first step ($K_{a,b}$) and the classical TST formula^{90–92} to calculate k_c

$$K_{a,b}(T) = \frac{Q_{\text{MCR}}(T)}{Q_{\text{R}}(T)} \exp\left(\frac{E_{\text{R}} - E_{\text{MCR}}}{k_{\text{B}}T}\right) \quad (\text{8})$$

$$k_c(T) = \Gamma(T) \times \frac{k_{\text{B}}T}{h} \times \frac{Q_{\text{TS}}(T)}{Q_{\text{MCR}}(T)} \times \exp\left(-\frac{E_{\text{TS}} - E_{\text{MCR}}}{k_{\text{B}}T}\right) \quad (\text{9})$$

where $Q_{\text{R}}(T)$, $Q_{\text{MCR}}(T)$, and $Q_{\text{TS}}(T)$ are the total partition functions of the reactants, the prereactive complex, and the TS at the temperature T , respectively. E_{R} , E_{MCR} , and E_{TS} are the total energies at 0 K including the zero-point energy corrections, whereas $\Gamma(T)$ indicates the transmission coefficient used for the tunneling correction at temperature T ; k_{B} and h are Boltzmann's constant and Planck's constant, respectively.

The reaction path degeneracy is not included in this expression since the rotational symmetry numbers are already introduced in the calculation of the partition functions. The calculation of the reaction rate constants using the TST formulation given by eq 9 requires the proper computation of partition functions of the prereactive complex and the TS.

The rate constants of the different abstraction pathways have been calculated in two different ways for comparison purposes. In the first one (complex mechanism), the two-step mechanism described above is assumed to hold and the rate constant is obtained according to eq 7. In the second one (direct mechanism), it is assumed that each pathway is elemental, the formation of the prereactive complex is ignored, and the rate constant is calculated as

$$k(T) = \Gamma(T) \times \frac{k_{\text{B}}T}{h} \times \frac{Q_{\text{TS}}(T)}{Q_{\text{R}}(T)} \times \exp\left(-\frac{E_{\text{TS}} - E_{\text{R}}}{k_{\text{B}}T}\right) \quad (\text{10})$$

It is important to note that these two expressions turn out to be identical except for the BSSE correction between reactants and the prereactive complex, which is taken into account in the complex mechanism, and the value of the tunneling factor $\Gamma(T)$, which depends on the activation barrier of the elemental process in which the atom is abstracted.

$\Gamma(T)$ is calculated as the ratio of the quantum mechanical to the classical barrier crossing rate, assuming an unsymmetrical one-dimensional Eckart function barrier.⁹³ This method approximates the potential by a one-dimensional function that is fitted to reproduce the zero-point energy corrected barrier, the enthalpy of reaction at 0 K, and the curvature of the potential curve at the transition state. The existence of the complex in the entrance channel means that there are several rotational and vibrational energy levels from where tunneling may occur. We have assumed in the complex mechanism that a thermal equilibrium distribution of rovibrational energy levels is maintained, which corresponds to the high-pressure limiting behavior, and that all these levels, from the bottom of the well of the complex up to the top of the barrier, contribute to tunneling. On the contrary, at low pressure limit, the lack of collisional stabilization causes that none of the reactant complexes can reach energies below the reactants, and the $\Gamma(T)$ value is the same as when tunneling is calculated from the isolated reactants. Accordingly, the difference between high (complex mechanism) and low (direct mechanism) pressure limit rate constants arise not only from the value of $\Gamma(T)$ but also from the BSSE correction, which is present in the calculation of $K_{a,b}$ (complex mechanism).

The GPOP program⁹⁴ was used to extract information from Gaussian output files, to estimate the Eckart tunneling corrections, and to do the rate constant calculations over the temperature range of interest.

3. RESULTS AND DISCUSSION

3.1. Geometries and Vibrational Frequencies. Table 2 lists the essential structural parameters and imaginary vibrational frequencies calculated for the transition states and molecular complexes at the MP2/cc-pVTZ level of theory. More detailed information regarding optimized geometric parameters (reactants and products), optimized Cartesian coordinates (transition states and molecular complexes), vibrational frequencies (reactants, transition states, molecular complexes, and products), literature enthalpy of formation at 298 K, and $\Gamma(T)$ and $K_{a,b}$ values calculated at six different temperatures are presented in Tables 1S–9S of the Supporting Information.

3.1.1. Transition States. The H-abstraction reaction from CH_2ICl by OH radicals is characterized by two different transition structures ($\text{TS}_{\text{Hab,Clside}}$ and $\text{TS}_{\text{Hab,Iside}}$) with an

Table 2. Essential Structural Parameters and Imaginary Vibrational Frequencies for Transition States and Molecular Complexes Calculated at the MP2/cc-pVTZ Level of Theory

H-abstraction pathway						
parameter	MCR _{Hab}		TS _{Hab}		MCP _{Hab}	
	Cl side	I side	Cl side	I side	Cl side	I side
$r(\text{C}-\text{H})$ (Å)	1.082	1.082	1.180	1.182	3.201	3.263
$r(\text{O}-\text{H})$ (Å)	2.552	2.552	1.321	1.318	0.960	0.961
θ (OHC) (deg)	119.6	119.6	164.6	171.0	98.8	84.1
L^a			0.271	0.279		
$\nu^\#$ (cm ⁻¹)			1899i	1960i		
Cl-abstraction pathway						
parameter	MCR _{Clab}		TS _{Clab}		MCP _{Clab}	
	Cl side	I side	Cl side	I side	Cl side	I side
$r(\text{C}-\text{Cl})$ (Å)		1.771		2.107		3.043
$r(\text{O}-\text{Cl})$ (Å)		3.396		1.728		1.700
θ (OClC) (deg)		69.2		157.5		175.3
L^a				10.7		
$\nu^\#$ (cm ⁻¹)				529i		
I-abstraction pathway						
parameter	MCR _{Iab}		TS _{Iab}		MCP _{Iab}	
	Cl side	I side	Cl side	I side	Cl side	I side
$r(\text{C}-\text{I})$ (Å)		2.125		2.485		3.047
$r(\text{O}-\text{I})$ (Å)		3.260		1.989		1.990
θ (OIC) (deg)		173.8		157.5		174.0
$\nu^\#$ (cm ⁻¹)				222i		

^aThe L parameter is defined as the ratio of the increase in the length of the bond being broken and the elongation of the bond being formed, each with respect to its equilibrium value in the reactant and the product.

intermolecular bond between the H atom from the hydroxyl radical and the halogen atom (either Cl or I). The intermolecular bond lengths $\text{H}\cdots\text{Cl}$ in $\text{TS}_{\text{Hab,Clside}}$ and $\text{H}\cdots\text{I}$ in $\text{TS}_{\text{Hab,Iside}}$ were estimated to be about 3.014 and 3.235 Å, respectively. Both transition structures exhibit a nearly linear OHC bond angle. The MP2/cc-pVTZ level of theory predicts a relatively early transition state on the potential energy surface, where the breaking C–H bond is stretched by only a small amount from its equilibrium value in CH_2ICl (1.082 Å), while the forming O–H bonds are still relatively long ($\text{TS}_{\text{Hab,Clside}}$: 1.321 Å; $\text{TS}_{\text{Hab,Iside}}$: 1.318 Å) compared to the equilibrium value in H_2O (0.967 Å). The main change in the geometrical structure of the transition state can be characterized by the L

parameter, defined as the ratio of the increase in the length of the bond being broken and the elongation of the bond being formed.⁹⁵ This parameter provides a reliable measure of the reactant- or product-like character of the concomitant transition state. Large L values correspond to product-like transition states, while smaller values correspond to reactant-like TSs. The calculated values of the L parameter are 0.271 and 0.279, which is much smaller than 1. The TS structures are indeed reactant-like. This is in agreement with Hammond's postulate,⁸⁸ which predicts a product-like character for the transition state when the reaction is endoergic and a reactant-like character with an exoergic reaction.

The Cl- or I-abstraction reaction from CH_2ICl by OH radicals is characterized by transition structures (TS_{Clab} and TS_{Iab}) with nearly linear OCIC and OIC bond angles. The MP2/cc-pVTZ level of theory predicts a relatively late transition state on the potential energy surface, where the breaking C–Cl and C–I bonds are stretched by a large amount (2.107 and 2.485 Å in TS_{Clab} and TS_{Iab} , respectively) from its equilibrium value in CH_2ICl (1.764 and 2.126 Å for the C–Cl and C–I bonds, respectively), while the forming O–X bonds are about the same (1.728 and 1.989 Å in TS_{Clab} and TS_{Iab} , respectively) as the equilibrium values in HOCl (1.696 Å) and HOI (1.992 Å).

In all transition states, the eigenvector in the vibrational mode corresponding to the imaginary frequency is primarily a motion of the atom being transferred (H, Cl, or I) between the C and the O centers.

3.1.2. Molecular Complexes. The IRC calculations at the MP2/cc-pVTZ level of theory have revealed that the minimum energy pathways connect the TSs to loosely bound van der Waals complexes in both the forward and backward directions.

3.1.2.1. H-Abstraction Pathway. $\text{TS}_{\text{Hab,Clside}}$ and $\text{TS}_{\text{Hab,Iside}}$ are connected to the $\text{HO}\cdots\text{HCHICl}$ reactant complexes ($\text{MCR}_{\text{Hab,Clside}}$ and $\text{MCR}_{\text{Hab,Iside}}$) and to the $\text{HOH}\cdots\text{CHICl}$ product complexes ($\text{MCP}_{\text{Hab,Clside}}$ and $\text{MCP}_{\text{Hab,Iside}}$). The structures of $\text{MCR}_{\text{Hab,Clside}}$, $\text{MCR}_{\text{Hab,Iside}}$, $\text{MCP}_{\text{Hab,Clside}}$, and $\text{MCP}_{\text{Hab,Iside}}$ are similar to that of $\text{TS}_{\text{Hab,Clside}}$ and $\text{TS}_{\text{Hab,Iside}}$ with two characteristic differences: (i) the emerging new bond O–H is much shorter in the transition state than in the MCR complexes (1.321 and 1.318 Å in $\text{TS}_{\text{Hab,Clside}}$ and $\text{TS}_{\text{Hab,Iside}}$ compared to 2.552 Å in $\text{MCR}_{\text{Hab,Clside}}$ and $\text{MCR}_{\text{Hab,Iside}}$, respectively) and (ii) the breaking bond C–H is much shorter in the transition states than in the MCP complexes (1.180 and

Table 3. Comparison of Various Energy Contributions to Enthalpies at 0 K Including Spin–Orbit Corrections (in kJ mol⁻¹) Calculated at the CCSD(T)/ANO-RCC-L(I)//MP2/cc-pVTZ^a Level of Theory for the H-Abstraction Pathways (Cl and I Sides)

H-abstraction pathway	forward				reverse				equilibrium
reaction step	OH + CH ₂ ICl → MCR _{Hab}		OH + CH ₂ ICl → TS _{Hab}		H ₂ O + CHICl → MCP _{Hab}		H ₂ O + CHICl → TS _{Hab}		OH + CH ₂ ICl = H ₂ O + CHICl
	ΔH_{0K}		ΔH_{0K}^\ddagger		ΔH_{0K}		ΔH_{0K}^\ddagger		$\Delta_r H_{0K}$
	Cl side	I side	Cl side	I side	Cl side	I side	Cl side	I side	
CCSD(T)	−14.92	−14.92	16.96	18.22	−9.85	−14.46	101.88	103.14	−84.92
ZPE correction	+3.69 ^b	+3.69	−7.20	−7.84	+3.02	+4.33	−5.62	−6.26	−1.58
SO correction	+0.99	+0.99	+1.39	+1.51	+0.15	+0.48	+0.58	+0.70	+0.81
cp correction	+2.73	+2.73	(+5.30) ^c	(+5.50) ^c	+2.75	+2.89	(+8.36) ^c	(+8.46) ^c	
cf correction	+1.74	+1.74	+0.89	+0.87	+2.66	+2.67	+2.23	+2.21	−1.34
CCSD(T) _{total} ^d	−5.77	−5.77	12.04	12.76	−1.27	−4.09	99.07	99.79	−87.03

^acc-pVTZ-PP on iodine atom, used within MP2 optimizations. ^bValues in italics are individual corrections to ΔH_{0K} and ΔH_{0K}^\ddagger . ^cAn estimate of the error bars based on counter-poise calculations for forward and reverse reactions. ^dTotal CCSD(T) value with the sum of individual corrections.

Table 4. Comparison of Various Energy Contributions to Enthalpies at 0 K Including Spin–Orbit Corrections (in kJ mol^{−1}) Calculated at the CCSD(T)/ANO-RCC-L(I)//MP2/cc-pVTZ^a Level of Theory for the Cl-Abstraction Pathway

Cl-abstraction pathway	forward		reverse		equilibrium
reaction step	OH + CH ₂ Cl → MCR _{Clab}	OH + CH ₂ Cl → TS _{Clab}	HOCl + CH ₂ I → MCP _{Clab}	HOCl + CH ₂ I → TS _{Clab}	OH + CH ₂ Cl = HOCl + CH ₂ I
	ΔH_{0K}	ΔH_{0K}^\ddagger	ΔH_{0K}	ΔH_{0K}^\ddagger	$\Delta_r H_{0K}$
CCSD(T)	−14.92	115.60	−9.83	12.57	103.03
ZPE correction	+3.70 ^b	+5.78	+2.92	+9.90	−4.11
SO correction	+1.00	+1.33	+1.58	+0.56	+0.77
cp correction	+2.54	(+4.98) ^c	+1.87	(+4.41) ^c	
cf correction	+1.74	+0.15	+0.83	−0.28	+0.43
CCSD(T) _{total} ^d	−5.94	122.86	−2.63	22.75	100.12

^acc-pVTZ-PP on iodine atom, used within MP2 optimizations. ^bValues in italics are individual corrections to ΔH_{0K} and ΔH_{0K}^\ddagger . ^cAn estimate of the error bars based on counter-poise calculations for forward and reverse reactions. ^dTotal CCSD(T) value with the sum of individual corrections.

Table 5. Comparison of Various Energy Contributions to Enthalpies at 0 K Including Spin–Orbit Corrections (in kJ mol^{−1}) Calculated at the CCSD(T)/ANO-RCC-L(I)//MP2/cc-pVTZ^a Level of Theory for the I-Abstraction Pathway

I-abstraction pathway	forward		reverse		equilibrium
reaction step	OH + CH ₂ Cl → MCR _{Iab}	OH + CH ₂ Cl → TS _{Iab}	HOI + CH ₂ Cl → MCP _{Iab}	HOI + CH ₂ Cl → TS _{Iab}	OH + CH ₂ Cl = HOI + CH ₂ Cl
	ΔH_{0K}	ΔH_{0K}^\ddagger	ΔH_{0K}	ΔH_{0K}^\ddagger	$\Delta_r H_{0K}$
CCSD(T)	−8.70	6.15	−17.66	−11.73	17.88
ZPE correction	+2.06 ^b	+6.26	+6.27	+10.73	−4.47
SO correction	+0.47	−0.63	+0.31	+1.77	−2.40
cp correction	+1.94	(+6.57) ^c	+3.40	(+5.74) ^c	
cf correction	+1.79	+0.55	+0.39	−0.29	+0.83
CCSD(T) _{total} ^d	−2.44	12.33	−7.29	0.48	11.84

^acc-pVTZ-PP on iodine atom, used within MP2 optimizations. ^bValues in italics are individual corrections to ΔH_{0K} and ΔH_{0K}^\ddagger . ^cAn estimate of the error bars based on counter-poise calculations for forward and reverse reactions. ^dTotal CCSD(T) value with the sum of individual corrections.

1.182 Å in TS_{Hab,Clside} and TS_{Hab,Iside} compared to 3.201 and 3.263 Å in MCR_{Hab,Clside} and MCR_{Hab,Iside} respectively).

3.1.2.2. Cl-Abstraction Pathway. TS_{Clab} is connected to the HO···ClCH₂I reactant complex (MCR_{Clab}) and to the HOCl···CH₂I product complex (MCP_{Clab}). When the oxygen atom from the hydroxyl radical approaches the chloriodomethane, it forms an intermolecular bond Cl–O of 3.396 Å. On the product side, the structure of MCP_{Clab} has been determined with an intermolecular bond C–Cl of 3.043 Å.

3.1.2.3. I-Abstraction Pathway. TS_{Iab} is connected to the HO···ICH₂Cl reactant complex (MCR_{Iab}) and to the HOI···CH₂Cl product complex (MCP_{Iab}). When the oxygen atom from the hydroxyl radical approaches the chloriodomethane, it forms an intermolecular bond I–O of 3.260 Å. On the product side, the structure of MCP_{Iab} has been determined with an intermolecular bond C–I of 3.047 Å.

3.2. Energetics. The electronic binding energies for molecular complexes, barriers, and overall reaction energies are collected in Tables 3–5 for the H-, Cl-, and I-abstraction pathways, respectively (indices cp and cf stand for counterpoise and continued-fraction corrections, respectively). First, let us mention that, in all single-point energy calculations, the absolute values of the single- and double-excitation amplitudes were below 0.1, confirming the applicability of the CCSD(T) single-reference based ROHF approach. The addition of ZPE and spin–orbit corrections to the electronic energies does show uniform trends. As shown in Tables 3–5, they tend to destabilize slightly the molecular complexes (H-, Cl-, and I-abstraction pathways) and the transition states (Cl- and I-abstraction pathways). The destabilization ranges, for example, from 2.53 kJ mol^{−1} (MCR_{Iab} complex formation) to 12.50 kJ

mol^{−1} (reverse activation barrier in the I-abstraction pathway). Concerning the two transition states involved in the H-abstraction pathway, the opposite trend is observed with stabilization effects ranging from −6.33 kJ mol^{−1} (forward activation barrier on the I side) to −5.04 kJ mol^{−1} (reverse activation barrier on the Cl side).

The compensation of the BSSE including geometry relaxation is only modest (in the range of 1.87 to 3.40 kJ mol^{−1}), below the required chemical accuracy threshold. It indicates that the ANO-RCC basis set is quite close to saturation, at least for the application in the reactivity of iodine related species. Goodson's extrapolations recipe to FCI modifies all the elementary steps slightly; however, the respective cf-contributions are non-negligible for the overall energy budget because they all oscillate between −1 and +3 kJ mol^{−1}, destabilizing both the molecular complexes and transition states. Nevertheless, it is important to minimize all errors because the cumulative effects of missing corrections could deteriorate the prediction of the binding energies in MCR and MCP complexes.

The reaction enthalpies $\Delta_r H_{298K}^\circ$ for each abstraction pathway have been also calculated using the literature heats of formation $\Delta_f H_{298K}^\circ$ of the species of interest (see Table 8S, Supporting Information, for data and relevant references). Two recent values have been reported in the literature concerning the standard enthalpy of formation at 298 K for CH₂Cl: the first one ((10.7 ± 1.9) kJ mol^{−1}) was derived from experimental studies using threshold photoelectron photoion coincidence spectroscopy,⁹⁶ while the other one (13.0 kJ mol^{−1}) was calculated at the MP2/3-21++G(2d,2p) level of theory by Kambanis and co-workers.⁴⁵ Using the experimental

Table 6. Rate Constants in $\text{cm}^3 \text{ molecule}^{-1} \text{ s}^{-1}$ Calculated at Six Different Temperatures at the CCSD(T)/ANO-RCC-L(I)//MP2/cc-pVTZ^a Level of Theory for H-, Cl-, and I-Abstraction Pathways and the Overall Reaction $\text{OH} + \text{CH}_2\text{ICl}$ Using Complex and Direct Mechanisms

rate constant complex mechanism	temperature (K)					
	250	300	350	400	450	500
H-abstraction Cl side	1.61×10^{-14}	1.94×10^{-14}	2.55×10^{-14}	3.45×10^{-14}	4.71×10^{-14}	6.37×10^{-14}
H-abstraction I side	1.95×10^{-14}	2.36×10^{-14}	3.12×10^{-14}	4.26×10^{-14}	5.85×10^{-14}	7.99×10^{-14}
Cl-abstraction	1.96×10^{-39}	4.38×10^{-35}	5.94×10^{-32}	1.39×10^{-29}	9.96×10^{-28}	3.13×10^{-26}
I-abstraction	2.19×10^{-16}	7.45×10^{-16}	1.86×10^{-15}	3.84×10^{-15}	6.93×10^{-15}	1.14×10^{-14}
overall	3.59×10^{-14}	4.37×10^{-14}	5.85×10^{-14}	8.10×10^{-14}	1.13×10^{-13}	1.55×10^{-13}

rate constant direct mechanism	temperature (K)					
	250	300	350	400	450	500
H-abstraction Cl side	1.68×10^{-14}	2.51×10^{-14}	3.66×10^{-14}	5.19×10^{-14}	7.17×10^{-14}	9.69×10^{-14}
H-abstraction I side	1.95×10^{-14}	2.96×10^{-14}	4.38×10^{-14}	6.30×10^{-14}	8.82×10^{-14}	1.21×10^{-13}
Cl-abstraction	6.60×10^{-39}	1.21×10^{-34}	1.42×10^{-31}	2.98×10^{-29}	1.97×10^{-27}	5.77×10^{-26}
I-abstraction	5.20×10^{-16}	1.54×10^{-15}	3.50×10^{-15}	6.69×10^{-15}	1.14×10^{-14}	1.78×10^{-14}
overall	3.68×10^{-14}	5.63×10^{-14}	8.39×10^{-14}	1.22×10^{-13}	1.71×10^{-13}	2.35×10^{-13}

^acc-pVTZ-PP on iodine atom, used within MP2 optimizations.

value⁹⁶ for $\Delta_r H^\circ_{298\text{K}}(\text{CH}_2\text{ICl})$, the corresponding $\Delta_r H^\circ_{298\text{K}}$ literature values are (-81.8 ± 3.2) , (90.7 ± 5.2) , and (6.1 ± 9.5) kJ mol^{-1} for the H-, Cl-, and I-abstraction pathways, respectively. The computed reaction enthalpies at the CCSD(T)/ANO-RCC-L(I)//MP2/cc-pVTZ level of theory including all corrections are close to the literature values especially when considering the associated uncertainties.

3.3. Kinetic Parameters Calculations. The calculations of the temperature dependence of rate constants have been performed at the CCSD(T)/ANO-RCC-L(I)//MP2/cc-pVTZ level of theory including four corrections (ZPE, SO, cp, and cf) for all abstraction pathways using the two mechanisms (complex and direct abstraction as discussed in section 2). Table 6 gathers our calculated values at six different temperatures (250, 300, 350, 400, 450, and 500 K). As shown in Table 6, there are differences between the rate constants calculated using the complex mechanism and those obtained by the direct abstraction mechanism. The calculated $\Gamma(T)$ using complex and direct mechanisms are listed in the in the Table 9S of the Supporting Information. The influence of the BSSE correction on the $K_{\text{a,b}}$ value is also gathered in Table 9S, Supporting Information. On one hand, it can be noticed that the BSSE correction itself tends to decrease the effective rate constant k by about one-third at 250 K to one-half at 500 K. On the other hand, it can be noticed that the $\Gamma(T)$ values calculated using the complex mechanism are greater than the ones obtained using the direct abstraction mechanism. It is worth noticing that biggest differences (higher than a factor of 2) are observed for the H-abstraction pathway (Cl and I sides) at the lowest temperatures ($T < 300$ K). Differences between calculated rate constants using the two approaches (complex and direct mechanisms) are rather moderate (about 20 to 30% over the temperature range 300–500 K) and below the expected accuracy of rate constant calculations. As it can be seen in Table 6, the Cl-abstraction pathway is not relevant over the whole studied temperature range. For an abstraction reaction between OH radicals and CH_2ICl , we can define the branching ratio $f_{\text{X}}^{\text{CH}_2\text{ICl}}$ (in %) as the ratio of the rate constant for the X-abstraction pathway to that of the overall rate constant of the reaction. The branching ratios of H-abstraction (Cl and I sides) and I-abstraction channels calculated using complex and direct mechanisms over the temperature range

250–500 K are gathered in Table 7. Differences between calculated branching ratios using the two approaches (complex

Table 7. Branching Ratios $f_{\text{X}}^{\text{CH}_2\text{ICl}}$ in % Calculated at six Different Temperatures at the CCSD(T)/ANO-RCC-L(I)//MP2/cc-pVTZ^a Level of Theory for the H- and I-abstraction Pathways Using Complex and Direct Mechanisms^b

branching ratio	temperature (K)					
	250	300	350	400	450	500
$f_{\text{Hab,Cl side}}^{\text{CH}_2\text{ICl}}$	44.98	44.36	43.54	42.67	41.84	41.12
$f_{\text{Hab,I side}}^{\text{CH}_2\text{ICl}}$	46.71	44.63	43.60	42.67	42.25	41.18
$f_{\text{Iab}}^{\text{CH}_2\text{ICl}}$	54.41	53.93	53.27	52.59	52.00	51.53
$f_{\text{Iab}}^{\text{CH}_2\text{ICl}}$	52.82	52.62	52.23	51.83	51.50	51.24
$f_{\text{Iab}}^{\text{CH}_2\text{ICl}}$	0.61	1.71	3.19	4.74	6.16	7.35
$f_{\text{Iab}}^{\text{CH}_2\text{ICl}}$	1.41	2.74	4.17	5.50	6.64	7.54

^acc-pVTZ-PP on iodine atom, used within MP2 optimizations.

^bValues calculated for the direct mechanism are in italics.

and direct mechanisms) are rather small. At typical atmospheric temperatures, we found that the I-abstraction exhibit very low $f_{\text{Iab}}^{\text{CH}_2\text{ICl}}$ values (a few %) indicating that it is a minor pathway. For CH_2ICl , the H-abstraction is consistently the most important channel over the whole temperature range. It is also worth noticing that the two pathways (Hab,Cl side and Hab,I side) are both competitive. The overall rate constant for the reaction of OH radicals with CH_2ICl corresponds therefore to the sum of individual relevant pathways: H-abstraction on Cl side, H-abstraction on I side, and I-abstraction. The computed overall rate constant values are also given in Table 6, while Figure 2 depicts the temperature dependence of the rate constants for all major reactions reaction pathways together with the overall values.

The modified three-parameter Arrhenius expressions $k(T) = BT^m \exp(-E_a/RT)$ fitted to the overall rate constant computed over the temperature range 250–500 K (in $\text{cm}^3 \text{ molecule}^{-1} \text{ s}^{-1}$) are as follows:

complex mechanism

$$k = 2.03 \times 10^{-30} T^{5.84} \exp(1287/T)$$

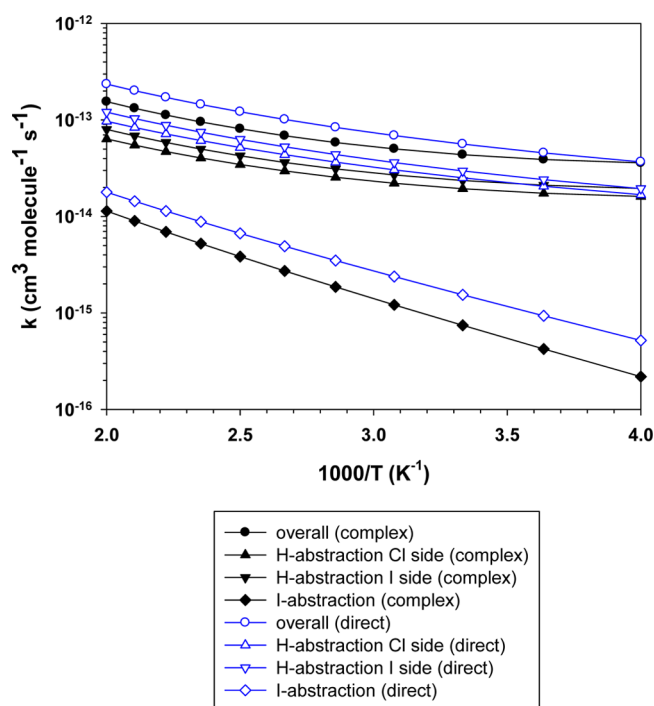


Figure 2. Temperature dependence of the rate constants of the overall reaction of OH radicals with CH_2ICl together with those of the major reaction pathways (H-abstraction on Cl and I sides, I-abstraction) calculated using complex and direct mechanisms.

direct mechanism

$$k = 2.08 \times 10^{-24} T^{3.95} \exp(442/T)$$

Using the above Arrhenius expression, the rate constants computed at 298 K are 4.29×10^{-14} and 5.44×10^{-14} $\text{cm}^3 \text{ molecule}^{-1} \text{ s}^{-1}$ for complex and direct mechanisms, respectively. Our result is in agreement with the upper limit value ($<10^{-13}$ $\text{cm}^3 \text{ molecule}^{-1} \text{ s}^{-1}$), which was estimated by Orlando¹⁸ in his review dealing with the atmospheric chemistry of organic bromine and iodine compounds.

3.4. Atmospheric Lifetimes. Reactions with hydroxyl radicals in the troposphere constitute the main removal pathways of hydrogen-containing compounds. Following Prather and Spivakovsky,⁹⁷ we can estimate the atmospheric lifetime of CH_2ICl due to its reaction with hydroxyl radicals in the troposphere as

$$\tau_{\text{CH}_2\text{ICl}}^{\text{OH}} = \frac{k_{\text{CH}_3\text{CCl}_3}^{\text{OH}}(277\text{K})}{k_{\text{CH}_2\text{ICl}}^{\text{OH}}(277\text{K})} \times \tau_{\text{CH}_3\text{CCl}_3}^{\text{OH}} \quad (11)$$

where $\tau_{\text{CH}_2\text{ICl}}^{\text{OH}}$ and $\tau_{\text{CH}_3\text{CCl}_3}^{\text{OH}}$ are the atmospheric lifetimes of CH_2ICl and methyl chloroform (CH_3CCl_3), respectively, due to reactions with hydroxyl radicals in the troposphere only. In eq 11, $k_{\text{CH}_2\text{ICl}}^{\text{OH}}(277\text{K})$ and $k_{\text{CH}_3\text{CCl}_3}^{\text{OH}}(277\text{K})$ are the rate constants for the reactions of OH with these compounds at $T = 277\text{K}$. Calculated $k_{\text{CH}_2\text{ICl}}^{\text{OH}}(277\text{K})$ values are (in $\text{cm}^3 \text{ molecule}^{-1} \text{ s}^{-1}$) either 3.88×10^{-14} using the complex mechanism or 4.56×10^{-14} using the direct mechanism. The corresponding rate constant for the reaction of OH with CH_3CCl_3 is 6.79×10^{-15} $\text{cm}^3 \text{ molecule}^{-1} \text{ s}^{-1}$. This latter value was taken from the JPL 10-6 Data Evaluation.⁹⁸

A value of $\tau_{\text{CH}_3\text{CCl}_3}^{\text{OH}}$ equal to 5.9 years was used, which was obtained following the procedure used by Prinn et al.⁹⁹ from

the measured lifetime of CH_3CCl_3 , $\tau_{\text{CH}_3\text{CCl}_3} = 4.8$ years, taking into account partial lifetimes due to ocean loss of 85 years and to stratospheric loss of 37 years.

Table 8 shows the results of this prediction as well as those obtained for a set of dihalomethanes of type CH_2XY by Louis

Table 8. Atmospheric Lifetimes in Years for a Series of Dihalomethanes of Type CH_2XY

compound	$\tau_{\text{CH}_2\text{XY}}^{\text{OH}}$ (theory)	$\tau_{\text{CH}_2\text{XY}}^{\text{OH}}$ (expt) ^a
CH_2F_2	3.59 Louis et al. ¹⁰⁰	5.30 Sander et al. ⁹⁸
CH_2FCl	1.68 Louis et al. ¹⁰⁰	1.32 Sander et al. ⁹⁸
CH_2FBr	6.03 Louis et al. ¹⁰⁰	unknown
CH_2Cl_2	0.43 Louis et al. ¹⁰⁰	0.49 Sander et al. ⁹⁸
CH_2ClBr	0.54 Louis et al. ¹⁰⁰	0.46 Sander et al. ⁹⁸
CH_2Br_2	0.57 Louis et al. ¹⁰⁰	0.42 Sander et al. ⁹⁸
CH_2ICl	1.03 this work	unknown
	<i>0.88^b</i>	

^aExperimental values of the rate constants at 277 K are calculated from the Arrhenius expressions reported in ref 98. ^bValue calculated for the direct mechanism is in italics.

et al.¹⁰⁰ For the reaction of OH with CH_2ICl , we estimate the atmospheric lifetime to be either 1.03 years using the complex mechanism or 0.88 years using the direct mechanism. These values are greater by about a factor of 2 than those estimated for CH_2Cl_2 , CH_2ClBr , and CH_2Br_2 . Note that the estimates of the lifetimes of these compounds do not include loss mechanisms due to photolysis or reaction with Cl atoms. Any contribution from these sources will indeed lead to a lower actual lifetime. For the photolysis, Orlando¹⁸ estimated the atmospheric lifetime to be 0.12 days, while for the reaction of chlorine atoms with CH_2ICl , the atmospheric lifetimes have been estimated to be 135 and 2.7 days in a global atmosphere and in the marine boundary layer, respectively. In the absence of any available experimental data, the results of our theoretical calculations confirm that, in the case of CH_2ICl , the OH reaction is not competitive with Cl reaction and photolysis.

4. CONCLUSIONS

We have studied gas-phase chemical reactivity of OH toward CH_2ICl using high-level ab initio methods. The stationary points on the energy profiles determined at the MP2/cc-pVTZ level were recalculated using the DK-CCSD(T)/ANO-RCC level with two types of contractions for the basis sets (quadruple- ζ for H, C, O, and Cl atoms; large for I atom) and corrected for the BSSE using the OVOS technique as well as refined with the extrapolation to FCI using the continued-fraction approximation. This approach was tested for iodine chemistry previously^{47,82,83} and leads to predictions within chemical accuracy.

These single-point energy calculations revealed the following: (1) The all-electron DK-CCSD(T)/ANO-RCC approach performs very well in predicting the reactivity of iodine. (2) The energy profile for the Cl-abstraction, in contrast to the H- and I-abstractions, exhibits a large activation enthalpy at 0 K indicating that this reaction pathway is not energetically favorable. In the case of the H- and I-abstractions, both pathways are competitive. (3) The H-abstraction is strongly exothermic (-87 kJ mol^{-1}), while the I-abstraction is modestly endothermic (11.8 kJ mol^{-1}). This is predominantly pertinent to the difference in C–H and C–I bond strengths (431 versus

239 kJ mol⁻¹).¹⁰¹ (4) Predicted rate constants based on canonical transition state theory including an asymmetrical Eckart tunneling correction are computed using two different approaches (complex and direct mechanisms) for each abstraction pathway over the temperature range 250–500 K. The overall rate constant at 298 K is estimated to be 4.29×10^{-14} and 5.44×10^{-14} cm³ molecule⁻¹ s⁻¹ for complex and direct mechanisms, respectively. Both results are in agreement with literature estimation made by Orlando¹⁸ in his review ($<10^{-13}$ cm³ molecule⁻¹ s⁻¹). (5) On the basis of our calculations, the atmospheric lifetime for the OH removal process is predicted to be close to 1 year. In terms of atmospheric lifetime, the OH reaction is not competitive with the Cl reaction and photolysis processes.

■ ASSOCIATED CONTENT

■ Supporting Information

Optimized geometry parameters for reactants and products at the MP2/cc-pVTZ level of theory (Tables 1S,2S), optimized Cartesian coordinates for transition states and molecular complexes (Table 3S), calculated unscaled vibrational frequencies at the MP2/cc-pVTZ level of theory (Tables 4S,7S), literature standard enthalpy of formation at 298 K (Table 8S), and $\Gamma(T)$ and $K_{a,b}$ values calculated at six different temperatures (Table 9S). This material is available free of charge via the Internet at <http://pubs.acs.org>.

■ AUTHOR INFORMATION

Corresponding Author

*E-mail: florent.louis@univ-lille1.fr (F.L.); neogrady@fns.uniba.sk (P.N.).

Notes

The authors declare no competing financial interest.

■ ACKNOWLEDGMENTS

We thank the Centre de Ressources Informatiques de Haute Normandie (CRIHAN), and the Centre de Ressources Informatiques (CRI) of the University of Lille1 for providing computing time for part of the theoretical calculations. We appreciate the support from Slovak Grant Agencies VEGA (Grant 1/0428/09) and APVV (Grant APVV-0059-10) and from the Research & Development Operational Program funded by the ERDF: Amplification of the Centre of Excellence on Green Chemistry Methods and Processes (CEGreen-II 26240120025). We thank Dr. Sébastien Canneaux (Université Lille1 Sciences et Technologies, Villeneuve d'Ascq, France) and Professor Ivan Černušák (Comenius University, Bratislava, Slovakia) for fruitful discussion.

■ REFERENCES

- (1) Lovelock, J. E.; Maggs, R. J.; Wade, R. J. Halogenated Hydrocarbons in and over the Atlantic. *Nature* **1973**, *241* (5386), 194–196.
- (2) Vogt, R. Iodine Compounds in the Atmosphere. In *Reactive Halogen Compounds in the Atmosphere*, Fabian, P., Singh, N. O., Eds; The Handbook of Environmental Chemistry; Springer-Verlag: Berlin, Germany, 1999; Vol. 4E, pp 113–128.
- (3) Cicerone, R. J. Halogens in the Atmosphere. *Rev. Geophys. Space Phys.* **1981**, *190*, 123–139.
- (4) Chameides, W. L.; Davis, D. D. Iodine: It's Possible Role in Tropospheric Photochemistry. *J. Geophys. Res., [Oceans]* **1980**, *85*, 7383–7398.
- (5) Carpenter, L. J. Iodine in the Marine Boundary Layer. *Chem. Rev.* **2003**, *103* (12), 4953–4962.
- (6) Saiz-Lopez, A.; Plane, J. M. C.; Baker, A. R.; Carpenter, L. J.; von Glasow, R.; Gómez Martín, J. C.; McFiggans, G.; Saunders, R. W. Atmospheric Chemistry of Iodine. *Chem. Rev.* **2012**, *112* (3), 1773–1804.
- (7) Class, T.; Kohnle, R.; Ballschmiter, K. Chemistry of Organic Traces in Air VII: Bromo- and Bromochloromethanes in Air over the Atlantic Ocean. *Chemosphere* **1986**, *15* (4), 429–436.
- (8) Class, T.; Ballschmiter, K. Chemistry of Organic Traces in Air. *J. Atmos. Chem.* **1988**, *6* (1), 35–46.
- (9) Klick, S.; Abrahamsson, K. Biogenic Volatile Iodated Hydrocarbons in the Ocean. *J. Geophys. Res.* **1992**, *97* (C8), 12683–12687.
- (10) Moore, R. M.; Tokarczyk, R. Chloro-Iodomethane in N. Atlantic Waters: A Potentially Significant Source of Atmospheric Iodine. *Geophys. Res. Lett.* **1992**, *19* (17), 1779–1782.
- (11) Carpenter, L. J.; Sturges, W. T.; Penkett, S. A.; Liss, P. S.; Alicke, B.; Hebestreit, K.; Platt, U. Short-Lived Alkyl Iodides and Bromides at Mace Head, Ireland: Links to Biogenic Sources and Halogen Oxide Production. *J. Geophys. Res.* **1999**, *104* (D1), 1679–1689.
- (12) Carpenter, L. J.; Liss, P. S.; Penkett, S. A. Marine Organohalogen in the Atmosphere over the Atlantic and Southern Oceans. *J. Geophys. Res.* **2003**, *108* (D9), 4256–4268.
- (13) Saiz-Lopez, A.; Plane, J. M. C. Novel Iodine Chemistry in the Marine Boundary Layer. *Geophys. Res. Lett.* **2004**, *31* (4), L04112.
- (14) Jones, C. E.; Carpenter, L. J. Solar Photolysis of CH₂I₂, CH₂ICl, and CH₂I₂Br in Water, Saltwater, and Seawater. *Environ. Sci. Technol.* **2005**, *39* (16), 6130–6137.
- (15) Jones, C. E.; Hornsby, K. E.; Dunk, R. M.; Leigh, R. J.; Carpenter, L. J. Coastal Measurements of Short-Lived Reactive Iodocarbons and Bromocarbons at Roscoff, Brittany during the RHaMBLe Campaign. *Atmos. Chem. Phys.* **2009**, *9* (22), 8757–8769.
- (16) Jones, C. E.; Hornsby, K. E.; Sommariva, R.; Dunk, R. M.; von Glasow, R.; McFiggans, G.; Carpenter, L. J. Quantifying the Contribution of Marine Organic Gases to Atmospheric Iodine. *Geophys. Res. Lett.* **2010**, *37* (18), L18804.
- (17) Martino, M.; Mills, G. P.; Woeltjen, J.; Liss, P. S. A New Source of Volatile Organoiodine Compounds in Surface Seawater. *Geophys. Res. Lett.* **2009**, *36* (1), L01609.
- (18) Orlando, J. Atmospheric Chemistry of Organic Bromine and Iodine Compounds. In *The Handbook of Environmental Chemistry*; Springer: Berlin, Germany, 2003; Vol. 3R, pp 253–299.
- (19) Redeker, K. R.; Wang, N.-Y.; Low, J. C.; McMillan, A.; Tyler, S. C.; Cicerone, R. J. Emissions of Methyl Halides and Methane from Rice Paddies. *Science* **2000**, *290* (5493), 966–969.
- (20) Andreae, M. O.; Atlas, E.; Harris, G. W.; Helas, G.; de Kock, A.; Koppmann, R.; Maenhaut, W.; Man, S.; Pollock, W. H. Methyl Halide Emissions from Savanna Fires in Southern Africa. *J. Geophys. Res.* **1996**, *101* (D19), 23603–23613.
- (21) Blake, N. J.; Blake, D. R.; Sive, B. C.; Chen, T.-Y.; Rowland, F. S.; Collins, J. E., Jr.; Sachse, G. W.; Anderson, B. E. Biomass Burning Emissions and Vertical Distribution of Atmospheric Methyl Halides and Other Reduced Carbon Gases in the South Atlantic Region. *J. Geophys. Res.* **1996**, *101* (D19), 24151–24164.
- (22) Andreae, M. O.; Merlet, P. Emission of Trace Gases and Aerosols from Biomass Burning, *Global Biogeochem. Cycles* **2001**, *15* (4), 955–966.
- (23) Rasmussen, R. A.; Khalil, M. A. K.; Gunawardena, R.; Hoyt, S. D. Atmospheric Methyl Iodide (CH₃I). *J. Geophys. Res.* **1982**, *87* (C4), 3086–3090.
- (24) Oram, D. E.; Penkett, S. A. Observations in Eastern England of Elevated Methyl Iodide Concentrations in Air of Atlantic Origin. *Atmos. Environ.* **1994**, *28* (6), 1159–1174.
- (25) Moore, R. M.; Zafiriou, O. C. Photochemical Production of Methyl Iodide in Seawater. *J. Geophys. Res.* **1994**, *99* (D8), 16415–16420.
- (26) Hapell, J. D.; Wallace, D. W. R. Methyl Iodide in the Greenland/Norwegian Seas and the Tropical Atlantic Ocean:

Evidence for Photochemical Production. *Geophys. Res. Lett.* **1996**, *23* (16), 2105–2108.

(27) Yokouchi, Y.; Nojiri, Y.; Barrie, L. A.; Toom-Sauntry, D.; Fujinuma, Y. Atmospheric Methyl Iodide: High Correlation with Surface Seawater Temperature and Its Implications on the Sea-to-Air Flux. *J. Geophys. Res.* **2001**, *106* (D12), 12661–12668.

(28) Singh, H. B.; Salas, L. J.; Stiles, R. E. Methyl Halides in and over the Eastern Pacific (40 N–32 S). *J. Geophys. Res.* **1983**, *88* (C6), 3684–3690.

(29) Reifenhäuser, W.; Heumann, K. G. Determinations of Methyl Iodide in the Antarctic Atmosphere and the South Polar Sea. *Atmos. Environ., Part A* **1992**, *26* (16), 2905–2912.

(30) Moore, R. M.; Groszko, W. Methyl Iodide Distribution in the Ocean and Fluxes to the Atmosphere. *J. Geophys. Res.* **1999**, *104* (C5), 11163–11171.

(31) Giese, B.; Laturnus, F.; Adams, F. C.; Wiencke, C. Release of Volatile Iodinated C1–C4 Hydrocarbons by Marine Macroalgae from Various Climate Zones. *Environ. Sci. Technol.* **1999**, *33* (14), 2432–2439.

(32) Davis, D.; Crawford, J.; Liu, S.; McKeen, S.; Bandy, A.; Thornton, D.; Rowland, F.; Blake, D. Potential Impact of Iodine on Tropospheric Levels of Ozone and Other Critical Oxidants. *J. Geophys. Res.* **1996**, *101*, 2135–2147.

(33) Solomon, S.; Garcia, R.; Ravishankara, A. On the Role of Iodine in Ozone Depletion. *J. Geophys. Res.* **1994**, *99* (D10), 20491–20499.

(34) Calvert, J. G.; Lindberg, S. E. Potential Influence of Iodine-Containing Compounds on the Chemistry of the Troposphere in the Polar Spring. I. Ozone Depletion. *Atmos. Environ.* **2004**, *38* (30), 5087–5104.

(35) Brown, A. C.; Canosamas, C. E.; Wayne, R. P. A Kinetic Study of the Reactions of OH with CH₃I and CF₃I. *Atmos. Environ., Part A* **1990**, *24* (2), 361–367.

(36) Gilles, M. K.; Turnipseed, A. A.; Talukdar, R. K.; Rudich, Y.; Villalta, P. W.; Huey, L. G.; Burkholder, J. B.; Ravishankara, A. R. Reactions of O(³P) with Alkyl Iodides: Rate Coefficients and Reaction Products. *J. Phys. Chem.* **1996**, *100* (33), 14005–14015.

(37) Cotter, E. S. N.; Canosa-Mas, C. E.; Manners, C. R.; Wayne, R. P.; Shallcross, D. E. Kinetic Study of the Reactions of OH with the Simple Alkyl Iodides: CH₃I, C₂H₅I, 1-C₃H₇I and 2-C₃H₇I. *Atmos. Environ.* **2003**, *37* (8), 1125–1133.

(38) Zhang, S.; Strekowski, R. S.; Monod, A.; Bosland, L.; Zetzsch, C. Temperature-Dependent Kinetics Study of the Reactions of OH with C₂H₅I, *n*-C₃H₇I, and *iso*-C₃H₇I. *J. Phys. Chem. A* **2012**, *116* (38), 9497–9506.

(39) Carl, S. A.; Crowley, J. N. 298 K Rate Coefficients for the Reaction of OH with *i*-C₃H₇I, *n*-C₃H₇I and C₃H₈. *Atmos. Chem. Phys.* **2001**, *1* (1), 1–7.

(40) Calvert, J. G.; Derwent, R. G.; Orlando, J. J.; Tyndall, G. S.; Wallington, T. J. *Mechanisms of Atmospheric Oxidation of the Alkanes*; Oxford University Press: New York: 2008.

(41) Brasseur, G. P.; Orlando, J. J.; Tyndall, G. S. *Atmospheric Chemistry and Global Change*; Oxford University Press: New York, 1999.

(42) Rattigan, O. V.; Shallcross, D. E.; Cox, R. A. UV Absorption Cross-Sections and Atmospheric Photolysis Rates of CF₃I, CH₃I, C₂H₅I and CH₂Cl. *J. Chem. Soc., Faraday Trans.* **1997**, *93* (16), 2839–2846.

(43) Roehl, C. M.; Burkholder, J. B.; Moortgat, G. K.; Ravishankara, A. R.; Crutzen, P. J. Temperature Dependence of UV Absorption Cross Sections and Atmospheric Implications of Several Alkyl Iodides. *J. Geophys. Res.* **1997**, *102* (D11), 12819–12829.

(44) Bilde, M.; Sehested, J.; Nielsen, O. J.; Wallington, T. J.; Meagher, R. J.; McIntosh, M. E.; Pietry, C. A.; Nicovich, J. M.; Wine, P. H. Kinetics and Mechanism of the Gas Phase Reaction of Atomic Chlorine with CH₂Cl at 206–432 K. *J. Phys. Chem. A* **1997**, *101* (43), 8035–8041.

(45) Kambanis, K. G.; Argyris, D. Y.; Lazarou, Y. G.; Papagiannakopoulos, P. Absolute Reaction Rate of Chlorine Atoms

with Chloriodomethane. *J. Phys. Chem. A* **1999**, *103* (17), 3210–3215.

(46) Feller, D.; Peterson, K. A.; de Jong, W. A.; Dixon, D. A. Performance of Coupled Cluster Theory in Thermochemical Calculations of Small Halogenated Compounds. *J. Chem. Phys.* **2003**, *118*, 3510–3522.

(47) Mečiarová, K.; Cantrel, L.; Černušák, I. Thermodynamic Data of Iodine Reactions Calculated by Quantum Chemistry. Training Set of Molecules. *Collect. Czech. Chem. Commun.* **2008**, *73* (10), 1340–1356.

(48) Möller, C.; Plesset, M. S. Note on an Approximation Treatment for Many-Electron Systems. *Phys. Rev.* **1934**, *46* (7), 618–622.

(49) Bartlett, R. J.; Stanton, J. F. Applications of Post-Hartree-Fock Methods: A Tutorial. In *Reviews in Computational Chemistry*; Lipkowitz, K. B., Boyd, D. B., Eds.; VCH Publishers, Inc.: New York, 1994; pp 65–169.

(50) Dunning, T. H., Jr. I. Gaussian Basis Sets for Use in Correlated Calculations. I. The Atoms Boron through Neon and Hydrogen. *J. Chem. Phys.* **1989**, *90*, 1007–1023.

(51) Peterson, K. A.; Shepler, B. C.; Figgen, D.; Stoll, H. On the Spectroscopic and Thermochemical Properties of ClO, BrO, IO, and Their Anions. *J. Phys. Chem. A* **2006**, *110* (51), 13877–13883.

(52) Frisch, M. J.; Trucks, G. W.; Schlegel, H. B.; Scuseria, G. E.; Robb, M. A.; Cheeseman, J. R.; Montgomery, J. A., Jr.; Vreven, T.; Kudin, K. N.; Burant, J. C.; et al. *Gaussian 03*, revision D.01; Gaussian, Inc.: Wallingford, CT, 2004.

(53) Johnson, R. D., III, Ed. NIST Computational Chemistry Comparison and Benchmark Database, NIST Standard Reference Database Number 101, Release 15b; see <http://cccbdb.nist.gov/>.

(54) Gonzalez, C.; Schlegel, H. B. An Improved Algorithm for Reaction Path Following. *J. Chem. Phys.* **1989**, *90* (4), 2154–2161.

(55) Gonzalez, C.; Schlegel, H. B. Reaction Path Following in Mass-Weighted Internal Coordinates. *J. Phys. Chem.* **1990**, *94* (14), 5523–5527.

(56) Huber, K. P.; Herzberg, G. *Molecular Spectra and Molecular Structure. IV. Constants of Diatomic Molecules*; Van Nostrand Co.: New York, 1979.

(57) Aquilante, F.; De Vico, L.; Ferre, H.; Ghigo, G.; Malmqvist, P.-A.; Neogrady, P.; Pedersen, T.; Pitonak, M.; Reiher, M.; Roos, B.; et al. MOLCAS 7: The next generation. *J. Comput. Chem.* **2010**, *31*, 224–247.

(58) Neogrady, P.; Urban, M.; Hubac, I. Spin Adapted Restricted Hartree-Fock Reference Coupled-Cluster Theory for Open-Shell Systems. *J. Chem. Phys.* **1994**, *100* (5), 3706–3716.

(59) Neogrady, P.; Urban, M. Spin-Adapted Restricted Hartree-Fock Reference Coupled-Cluster Theory for Open-Shell Systems: Non-iterative Triples for Noncanonical Orbitals. *Int. J. Quantum Chem.* **1995**, *55* (2), 187–203.

(60) Urban, M.; Kellö, V. Some Trends in Relativistic and Electron Correlation Effects in Electric Properties of Small Molecules. *Adv. Quantum Chem.* **2005**, *50*, 249–269.

(61) Ilias, M.; Kellö, V.; Urban, M. Relativistic Effects in Atomic and Molecular Properties. *Acta Phys. Slovaca* **2010**, *60* (3), 259–391.

(62) Douglas, M.; Kroll, N. M. Quantum Electrodynamical Corrections to Fine-Structure of Helium. *Ann. Phys.* **1974**, *82*, 89–155.

(63) Hess, B. A. Relativistic Electronic-Structure Calculations Employing a Two-Component No-Pair Formalism with External-Field Projection Operators. *Phys. Rev. A* **1986**, *33*, 3742–3748.

(64) Roos, B. O.; Lindh, R.; Malmqvist, P.-A.; Velyazov, V.; Widmark, P.-O. Main Group Atoms and Dimers Studied with a New Relativistic ANO Basis Set. *J. Phys. Chem. A* **2003**, *108* (15), 2851–2858.

(65) Boys, S. F.; Bernardi, F. The Calculation of Small Molecular Interactions by the Differences of Separate Total Energies. Some Procedures with Reduced Errors. *Mol. Phys.* **1970**, *19*, 553–566.

(66) Chalasinski, G.; Szczesniak, M. M. Origins of Structure and Energetics of van der Waals Clusters from ab Initio Calculations. *Chem. Rev.* **1994**, *94* (7), 1723–1765.

(67) Xantheas, S. S. On the Importance of the Fragment Relaxation Energy Terms in the Estimation of the Basis Set Superposition Error

Correction to the Intermolecular Interaction Energy. *J. Chem. Phys.* **1996**, *104* (21), 8821–8824.

(68) Lendvay, G.; Mayer, I. Some Difficulties in Computing BSSE-Corrected Potential Surfaces of Chemical Reactions. *Chem. Phys. Lett.* **1998**, *297* (5–6), 365–373.

(69) Kraus, M.; Pitoňák, M.; Hobza, P.; Urban, M.; Neogrády, P. Highly Correlated Calculations Using Optimized Virtual Orbital Space with Controlled Accuracy. Application to Counterpoise Corrected Interaction Energy Calculations. *Int. J. Quantum Chem.* **2012**, *112* (4), 948–959.

(70) Adamowicz, L.; Bartlett, R. J. Optimized Virtual Orbital Space for High-Level Correlated Calculations. *J. Chem. Phys.* **1987**, *86* (11), 6314–6324.

(71) Adamowicz, L.; Bartlett, R. J.; Sadlej, A. J. Optimized Virtual Orbital Space for High-Level Correlated Calculations. II. Electric Properties. *J. Chem. Phys.* **1988**, *88* (9), 5749–5758.

(72) Neogrády, P.; Pitoňák, M.; Urban, M. Optimized Virtual Orbitals for Correlated Calculations: An Alternative Approach. *Mol. Phys.* **2005**, *103* (15–16), 2141–2157.

(73) Edmiston, C.; Krauss, M. Pseudonatural Orbitals as a Basis for the Superposition of Configurations. I. He_2 . *J. Chem. Phys.* **1966**, *45* (5), 1833–1839.

(74) Barr, T. L.; Davidson, E. R. Nature of the Configuration-Interaction Method in ab Initio Calculations. I. Ne Ground State. *Phys. Rev. A* **1970**, *1* (3), 644–658.

(75) Sosa, C.; Geertsen, J.; Trucks, G. W.; Bartlett, R. J.; Franz, J. A. Selection of the Reduced Virtual Space for Correlated Calculations. An Application to the Energy and Dipole Moment of H_2O . *Chem. Phys. Lett.* **1989**, *159* (2–3), 148–154.

(76) Neogrády, P.; Pitoňák, M.; Granatier, J.; Urban, M. Coupled Cluster Calculations: OVOS As an Alternative Avenue Towards Treating Still Larger Molecules. In *Recent Progress in Coupled Cluster Methods. Theory and Applications*; Čársky, P., Paldus, J., Pittner, J., Eds; Challenges and Advances in Computational Chemistry and Physics; Springer: New York, 2010.

(77) Urban, M.; Pitoňák, M.; Neogrády, P. In *Lecture Series on Computer and Computational Science, Trends and Perspectives in Modern Computational Science*; Maroulis, G., Simos, T., Eds.; Brill Academic Publishers: Leiden, The Netherlands, 2006; pp 265–285.

(78) Šulka, M.; Pitoňák, M.; Neogrády, P.; Urban, M. Electron Affinity of the O_2 Molecule: CCSD(T) Calculations Using the Optimized Virtual Orbitals Space Approach. *Int. J. Quantum Chem.* **2008**, *108* (12), 2159–2171.

(79) Šulka, M.; Labanc, D.; Kováč, M.; Pitoňák, M.; Černušák, I.; Neogrády, P. Ab Initio Study of the Stability of Beryllium Clusters: Accurate Calculations for Be_2 – Be_6 . *J. Phys. B* **2012**, *45* (8), 085102.

(80) Goodson, D. Z. Extrapolating the Coupled-Cluster Sequence toward the Full Configuration-Interaction Limit. *J. Chem. Phys.* **2002**, *116* (16), 6948–6956.

(81) Jasper, A. W.; Klippenstein, S. J.; Harding, L. B. The Effect of Spin–Orbit Splitting on the Association Kinetics of Barrierless Halogen Atom–Hydrocarbon Radical Reactions. *J. Phys. Chem. A* **2010**, *114* (18), 5759–5768.

(82) Louis, F.; Černušák, I.; Canneaux, S.; Meciárová, K. Atmospheric Reactivity of CH_3I and CH_2I_2 with OH Radicals: A Comparative Study of the H- versus I-Abstraction. *Comput. Theor. Chem.* **2011**, *965*, 275–284.

(83) Meciárová, K.; Šulka, M.; Canneaux, S.; Louis, F.; Černušák, I. A Theoretical Study of the Kinetics of the Forward and Reverse Reactions $\text{HI} + \text{CH}_3 = \text{I} + \text{CH}_4$. *Chem. Phys. Lett.* **2011**, *517* (4–6), 149–154.

(84) Roos, B. O.; Malmqvist, P.-A. Relativistic Quantum Chemistry: the Multiconfigurational Approach. *Phys. Chem. Chem. Phys.* **2004**, *6* (11), 2919–2927.

(85) Hess, B. A.; Buenker, R. J.; Marian, C. M.; Peyerimhoff, S. D. Investigation of Electron Correlation on the Theoretical Prediction of Zero-Field Splittings of $^2\Pi$ Molecular States. *Chem. Phys. Lett.* **1982**, *89* (6), 459–462.

(86) Chase, M. W., Jr. NIST-JANAF Thermochemical Tables, *J. Phys. Chem. Ref. Data*, **1998**, Monograph No. 9.

(87) Stevens, J. E.; Cui, Q.; Morokuma, K. An ab Initio Investigation of Spin-Allowed and Spin-Forbidden Pathways of the Gas Phase Reactions of $\text{O}(^3\text{P}) + \text{C}_2\text{H}_5\text{I}$. *J. Chem. Phys.* **1998**, *108* (4), 1544–1551.

(88) Hammond, G. S. A Correlation of Reaction Rates. *J. Am. Chem. Soc.* **1955**, *77*, 334–338.

(89) Singleton, D. L.; Cvetanovic, R. J. Temperature Dependence of the Reaction of Oxygen Atoms with Olefins. *J. Am. Chem. Soc.* **1976**, *98* (22), 6812–6819.

(90) Eyring, H. The Activated Complex in Chemical Reactions. *J. Chem. Phys.* **1935**, *3* (2), 107–115.

(91) Johnston, H. S. *Gas Phase Reaction Rate Theory*; The Roland Press Co.: New York, 1966.

(92) Laidler, K. J. *Theories of Chemical Reaction Rates*; McGraw-Hill: New York, 1969.

(93) Eckart, C. The Penetration of a Potential Barrier by Electrons. *Phys. Rev.* **1930**, *35* (11), 1303.

(94) Miyoshi, A. *GPOP software*, revision 2010.02.14m6, 2012; see <http://www.frad.t.u-tokyo.ac.jp/~miyoshi/gpop/>.

(95) Rayez, M.-T.; Rayez, J.-C.; Sawerysyn, J.-P. Ab Initio Studies of the Reactions of Chlorine Atoms with Fluoro- and Chloro-Substituted Methanes. *J. Phys. Chem.* **1994**, *98* (44), 11342–11352.

(96) Lago, A. F.; Kercher, J. P.; Bödi, A.; Sztáray, B.; Miller, B.; Wurzelmann, D.; Baer, T. Dissociative Photoionization and Thermochemistry of Dihalomethane Compounds Studied by Threshold Photoelectron Photoion Coincidence Spectroscopy. *J. Phys. Chem. A* **2005**, *109* (9), 1802–1809.

(97) Prather, M.; Spivakovsky, C. M. Tropospheric OH and the Lifetimes of Hydrochlorofluorocarbons. *J. Geophys. Res.* **1990**, *95*, 18723–18729.

(98) Sander, S. P.; Abbatt, J. P. D.; Barker, J. R.; Burkholder, J. B.; Friedl, R. R.; Golden, D. M.; Huie, R. E.; Kolb, C. E.; Kurylo, M. J.; Moortgat, G. K.; et al. *Chemical Kinetics and Photochemical Data for Use in Atmospheric Studies. Evaluation No. 17*, JPL Publication 10-6; Jet Propulsion Laboratory: Pasadena, CA, 2011; see <http://jpldataeval.jpl.nasa.gov>.

(99) Prinn, R. G.; Weiss, R. F.; Miller, B. R.; Huang, J.; Alyea, F. N.; Cunnold, D. M.; Fraser, P. J.; Hartley, D. E.; Simmonds, P. G. Atmospheric Trends and Lifetime of CH_3CCl_3 and Global OH Concentrations. *Science* **1995**, *269* (5221), 187–192.

(100) Louis, F.; Gonzalez, C. A.; Huie, R. E.; Kurylo, M. J. An ab Initio Study of the Kinetics of the Reactions of Halomethanes with the Hydroxyl Radical. 3. Kinetic Parameters Predictions for the Potential Halon Replacements CH_2FBr , CHFBr_2 , CHFCIBr , CHCl_2Br , and CHClBr_2 . *J. Phys. Chem. A* **2001**, *105* (9), 1599–1604.

(101) McMillen, D. F.; Golden, D. M. Hydrocarbon Bond Dissociation Energies. *Annu. Rev. Phys. Chem.* **1982**, *33* (1), 493–532.